Simulating Near-Edge X-Ray Absorption Spectra with Conventional Functionals: An Orthogonality Constrained Density Functional Theory Study†

Wallace D. Derricotte,* Francesco A. Evangelista.

Received Xth XXXXXXXXXX 20XX, Accepted Xth XXXXXXXXX 20XX
First published on the web Xth XXXXXXXXXX 200X
DOI: 10.1039/b000000x

Near-edge X-ray absorption spectroscopy (NEXAS) has proven itself to be a robust technique to probe molecular electronic structure. The most dominant feature of the near-edge structure, the edge", is composed of excitations of tightly bound core electrons to valence orbitals. Several theoretical approaches have been applied to the calculation of core-valence excitations; density functional methods are an attractive option because of their cheap computational cost. Time-dependent density functional theory (TDDFT) is a rigorous extension of DFT and is commonly used to calculate electronic excitations. However, in conjunction with standard density functionals, TDDFT fails to capture the long-range character of core-valence excitations and yields an average excitation energy error of 20.15eV when compared to gas-phase NEXAS experiments. Orthogonality constrained density functional theory (OCDFT) is a time-independent, variational formulation of density functional theory (DFT) that imposes an orthogonality constraint between the ground/excited-state Kohn-Sham wavefunctions. It has been shown that OCDFT is effective in the treatment of charge transfer interactions, which makes it an excellent candidate to treat core electron excitations due to the spatial separation of core and valence orbitals. Here we quantify the spatial similarity of charge transfer and core excitations by examining the orbital overlap between core and valence orbitals. We also investigate the accuracy of OCDFT when applied to the calculation of X-ray absorption near-edge structure. OCDFT is assessed over a test set that includes 8 molecules with 25 unique core-electron excitations. When compared to experiment, we show that across four different basis sets (def2-TZVP, def2-QZVP, cc-pCVTZ, cc-pCVQZ) OCDFT yields a mean average difference of less than 1.5eV.

1 Introduction

The advent of synchrotron light sources created a strong resurgence of spectroscopy in the X-ray region[1]. Near edge X-ray absorption spectroscopy (NEXAS) is a useful experimental technique to probe the local electronic and geometrical structure in a variety of molecular environments. It has been successfully applied to large biological systems[2], small gas phase molecules[3], organic thin-films[4], and semiconducting materials[5]. This wide range of applications is possible because synchrotron light sources can span an energy range that goes from a few electron volts (eVs)[6] to hundreds of MeVs[7]. As NEXAS experiments are becoming increasingly more feasible, there is a growing need to perform first-principle studies to aid in the interpretation of their spectra. Calculations of NEXAS spectra are challenging, and require computational methods that explicitly account for the excitations of core-level electrons, electronic relaxation effects, and electron correlation[8]. Several approaches have shown promise in this area including: scaled-opposite-spin configuration interaction singles with perturbative doubles [SOS-CIS(D)][9], multiple scattering X_α methods[10], a maximum overlap ΔSCF approach[11], transition potential theory[12], coupled-cluster response theory[8], and time-dependent density functional theory (TDDFT)[13]. Among these methods TDDFT is a very attractive option because of its reduced computational cost and ability to calculate multiple excited

states.

Within the density functional theory framework, TDDFT is regarded as the method of choice to treat electronic excited states because it is a rigorous extension of the ground-state formalism[14]. When applied in conjunction with frequency-independent exchange-correlation potentials, TDDFT yields accurate excitation energies for low-lying excited states. Recent work by Silva-Junior et al.[15] benchmarked TDDFT ionization energies in a class of 28 organic molecules, their results show a mean average deviation (MAD) of 0.27eV for singlet states and 0.44eV for triplet states. However, when Besley et al[11]. applied TDDFT to higher-energy core excitations, conventional exchange-correlation functionals yielded a MAD of 20.2eV clearly showing that for this class of excitations, TDDFT grossly underestimates the experimental excitation energy. This failure is not surprising at all. It is well known that TDDFT struggles with the treatment of charge transfer excited states[16], and in core excitations there is usually a small amount of orbital overlap and a high degree of spatial separation between the orbitals involved. The inaccuracy of TDDFT in this scenario is caused by the incorrect asymptotic behavior of the exchange-correlation potential which does not decay as $-\frac{1}{r}$ and the self-interaction error in standard functionals that is made more apparent due to the large self-interaction associated with core orbitals. Any reasonable quantitative agreement is only attained by using a self-interaction correction (SIC)[17], or range separated hybrid functionals in which the amount of long and short range Hartree–Fock exchange is reparametrized[18,19]. This is often the limiting factor for studying the edge structure of many chemical systems since the optimal amount of Hartree–Fock exchange varies with each unique system being studied.[20–22]. Currently, there are no computational methods in the DFT framework that have been proven to accurately treat core-excitations with standard density functionals. A method that can systematically produce accurate core-excitation energies with traditional hybrid density functionals is highly desirable.

Orthogonality constrained density functional theory (OCDFT)[23] is a variational, time-independent formulation of excited state DFT that maintains the favorable accuracy/cost ratio of traditional DFT. Additionally, OCDFT has the ability to accurately compute charge transfer excitation energies regardless of the amount of Hartree-Fock exchange present in the exchange-correlation functional. Previous work in our research group proved OCDFT in conjunction with standard density functionals could accurately handle charge transfer phenomena in simple systems like H_2 and $[HeH]^+$ with comparable accuracy to a configuration interaction singles (CIS) calculation. Therefore, we expect that OCDFT will be applicable to the computation of core-excitation energies without optimizing multiple functional parameters. In its original formulation, OCDFT was unable to calculate multiple excited states[23], a feature that is routinely employed in standard TDDFT and CIS algorithms. One of our goals is to extend the formulation and allow for the calculation of multiple core-valence excited states

Here we report an investigation into the accuracy of OCDFT when applied to the calculation of X-ray absorption near-edge structure. The most dominant feature of this structure, the

"edge", is composed of the excitations of core-electrons from their tightly bound occupied orbitals to the unoccupied virtual space. In order for a method to properly replicate and analyze NEXAS spectra, it must demonstrate accuracy in describing core-electron excitations. To prove this, OCDFT in tandem with the standard and popular Becke three-parameter Lee-Yang-Parr (B3LYP) functional is assessed over a test set that includes 10 molecules with 43 unique core-electron excitations. The accuracy of the method is tested further by utilizing it in an investigation of the near-edge structure of adenine.

2 Theory

In this section we provide a brief summary of orthogonality constrained density functional theory along with the necessary extension to multiple excited states, for the full details of the OCDFT derivation we refer the reader to Ref. 23. OCDFT is a time-independent variational formulation of DFT that builds upon the approach developed by Ayers, Levy, and Nagy[24]. OCDFT supplements this formulation by implementing a Kohn-Sham (KS) scheme in which the KS energy functional is augmented with an orthogonality constraint between the ground state and excited state wavefunctions

$$\left\langle \Phi^{(1)} \middle| \Phi \right\rangle = 0, \tag{1}$$

where $\Phi^{(1)}$ is a Slater determinant wavefunction representing the first excited state built in the KS spin orbital basis $\{\phi_i^{(1)}\}$ and Φ is the ground state determinant. Imposing this constraint introduces an explicit hole orbital ($\phi_h^{(1)}$) and particle orbital ($\phi_p^{(1)}$) for the excited state. Where $\phi_h^{(1)}$ represents the orbital in the occupied space that the electron was promoted from and $\phi_p^{(1)}$ represents the orbital in the virtual space that the electron now occupies in the excited configuration. These orbitals naturally satisfy the following conditions

$$\hat{Q}\phi_h^{(1)} = 0, \tag{2}$$

$$\hat{P}\phi_p^{(1)} = 0, \tag{3}$$

where $\hat{P}$ and $\hat{Q}$ are projections onto the occupied and virtual space of $|\Phi\rangle$ respectively. By restricting the space spanned by $\phi_h^{(1)}$ and $\phi_p^{(1)}$, equations 2 and 3 are enforcing the fact that an electron can not be promoted from a virtual orbital or promoted to an occupied orbital. The projection operators are designed to span over the entire occupied and virtual space by taking the total summation of the outer products of every orbital contained in the set.

$$\hat{P} = \sum_i^{\text{occ}} |\phi_i\rangle\langle\phi_i|, \tag{4}$$

$$\hat{Q} = \sum_a^{\text{vir}} |\phi_a\rangle\langle\phi_a|. \tag{5}$$

The orthogonality condition is enforced explicitly for the hole orbital through the use of Lagrange multipliers. The resulting Lagrangian minimizes the excited state energy with respect to the orthogonality constraints

$$\begin{aligned}\mathscr{L}^{(1)}[\{\phi_i^{(1)}\},\phi_{\text{h}}^{(1)}] =& E_{\text{KS}}^{(1)}[\{\phi_i^{(1)}\}] + \sum_a^{\text{vir}} \lambda_a \langle \phi_{\text{h}}^{(1)} | \phi_a \rangle \\ & - \sum_{pq} \varepsilon_{pq}^{(1)} (\langle \phi_p^{(1)} | \phi_q^{(1)} \rangle - \delta_{pq}),\end{aligned} \tag{6}$$

The second term of the Lagrangian explicitly enforces the orthogonality constraint between the hole orbital and the ground

state virtual set that was introduced in equation 2, while the last term enforces the general orbital orthogonality condition between the excited state orbitals. $E_{KS}^{(1)}[\{\phi_i^{(1)}\}]$ is the standard KS energy functional for the excited state. Setting the variation of the Lagrangian with respect to $\{\phi_i^{(1)}\}$ and $\phi_h^{(1)}$ to zero results in a set of stationary conditions that lead to the following eigenvalue equation:

$$\hat{P}(1-\hat{Q}_s)\hat{f}|\phi_h^{(1)}\rangle = \varepsilon_h|\phi_h^{(1)}\rangle, \tag{7}$$

where $\hat{Q}_s$ is the projection onto the orbitals that are in the virtual space but not involved in the excitation, we refer to such orbitals as "spectators". These projection operators have an intuitive identity that for any excited state k, $\hat{P}$ and $\hat{Q}$ must sum to unity.

$$\hat{P}^{(k)} + \hat{Q}^{(k)} = 1. \tag{8}$$

This identity reveals the physical significance of the $1-\hat{Q}_s$ operator that appears in equation 7, as it can be interpreted as the projection onto the entire excitation space for a given state, a visual representation of this is shown in Figure 1. The algorithm detailed in equation 7 constrains the hole orbital basis, thus we refer to it as the constrained hole (CH) algorithm. It is possible to extend this formulation to multiple excited states by simply removing the hole belonging to the previous excited state from the spectator space

$$\hat{P}[1-\hat{Q}_s-(\hat{P}_{\mathrm{h}}^{(1)}+\hat{P}_{\mathrm{h}}^{(2)}+...+\hat{P}_{\mathrm{h}}^{(\mathrm{k}-1)})]\hat{f}|\phi_{\mathrm{h}}^{(\mathrm{k})}\rangle = \varepsilon_{\mathrm{h}}^{(\mathrm{k})}|\phi_{\mathrm{h}}^{(\mathrm{k})}\rangle. \tag{9}$$

Using this method extends the CH algorithm to allow the calculation of any excited state "k". We refer to this as the multi-

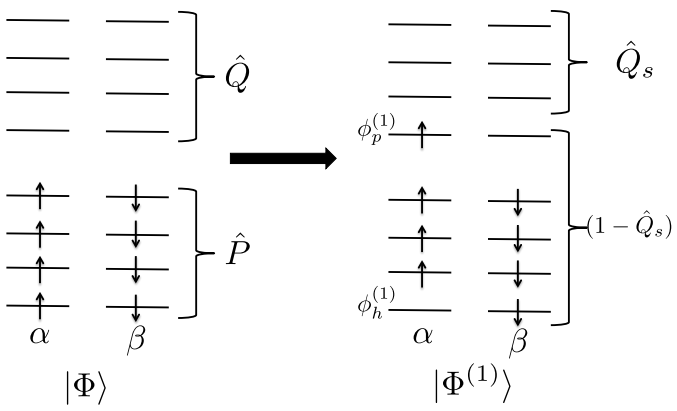

Fig. 1 Visual representation of the space spanned by all projection operators for the ground state determinant $|\Phi\rangle$ and the excited state determinant $|\Phi^{(1)}\rangle$. Notice that the hole orbital comes from the space spanned by $\hat{P}$ and that the particle orbital comes from the space spanned by $\hat{Q}$, this is a direct result of Equations 2 and 3.

constrained hole projection (MCHP) algorithm. It is important to note here that the ordering of the energy eigenvalues is not arbitrary, they are ordered by increasing orbital energy

$$\varepsilon_{\mathrm{h}}^{(1)} \leq \varepsilon_{\mathrm{h}}^{(2)} \leq \varepsilon_{\mathrm{h}}^{(3)} \leq ... \leq \varepsilon_{\mathrm{h}}^{(\mathrm{k})}. \tag{10}$$

Because of this, in order for the MCHP algorithm to obtain the energy for the k^{th} excited state, it must first project out all holes related to excited states $1 \rightarrow (k-1)$.

3 Computational Details

OCDFT was used to compute 40 unique core-excitations from a test set of 13 molecules. Its accuracy was assessed by comparing it to experimental data from gas-phase NEXAS experiments. Excitations from 1s orbitals are considered for all multi-electron atoms in each molecule, in addition to excitations from 2p orbitals for second row elements. All

structures were optimized using the Karlsruhe triple zeta valence polarization (def2-TZVP) basis set[25,26] available in the PSI4 *ab initio* quantum chemistry package[27]. Optimized geometries and excitation energies were computed consistently using the same functional and basis set.

The inclusion of scalar relativistic effects are a common practice when studying excitations of core electrons.[28–31] It was rigorously proven by Levy[32] that the excitation energy, ω, can be expressed in terms of ground state KS orbital energies (ε) in the following way

$$\omega = \varepsilon_{\mathrm{p}} - \varepsilon_{\mathrm{h}} + \Delta v_{\mathrm{xc}} \tag{11}$$

Where the p and h subscripts denote the particle and hole orbitals involved in the excitation and Δv_{xc} is the potential difference between the ground state and the excited state. Work by Desclaux et al.[33] shows that the largest orbital effect when solving the relativistic hartree-fock equations is the contraction of the 1s orbital, this contraction ($\gamma^{1\mathrm{s}}$) can be approximated by observing the energy reduction of the orbital between a nonrelativistic (NR) and relativistic (R) calculation as shown in Equation 12

$$\gamma^{1\mathrm{s}} = \varepsilon_{1\mathrm{s}}^{\mathrm{NR}} - \varepsilon_{1\mathrm{s}}^{\mathrm{R}} \, . \tag{12}$$

The relativistic orbital energies were obtained using the Douglass-Kroll Hess (DKH) Hamiltonian[34–36], and then the subsequent $\gamma^{1\mathrm{s}}$ is applied directly to the excitation energy

$$\omega = \varepsilon_{\mathrm{p}} - \varepsilon_{\mathrm{h}} + \Delta v_{\mathrm{xc}} + \gamma^{1\mathrm{s}}. \tag{13}$$

The relativistic contraction for first row 1s core orbitals are negligibly small (C, N, and O 1s contractions are approximately 0.1, 0.2, and 0.3 eV respectively). For second row nuclei, $\gamma^{1\mathrm{s}}$ was approximated to be 3.8, 6.8, 8.7, 6.8, 5.1, and 10.1 eV respectively for SiH_4 , H_2S, HCl, SO_2, PH_3, and Cl_2. Excitations from 2p orbitals were taken into consideration for all molecules containing second row nuclei, $\gamma^{2\mathrm{p}}$ was similar in magnitude to the negligibly small relativistic contractions seen in first row 1s orbitals. Therefore in this current study, we only consider scalar relativistic effects for second row 1s nuclei.

4 Results and Discussion

In this section we present core-excitation energies calculated using OCDFT for a benchmarking test set that consists of excitations from first row and second row elements. We also compute the carbon and nitrogen K-edge structure of thymine and adenine to display that OCDFT can accurately reproduce spectral details without the aid of an arbitrary shift of the spectra, as is common practice with TDDFT methods.[37,38] Previous studies done using time dependent density functional methods have all concluded that the 20-25% hartree-fock exchange present in many standard hybrid functionals is not sufficient enough to describe core-excited states using TDDFT. We aim to show here that OCDFT does not have such a strong dependance on the amount of hartree-fock exchange present in the functional. In order to show this, we will compute core-excited states using two standard hybrid functionals, B3LYP (20% HF exchange) and PBE0 (25% HF exchange). As well as a pure functional, BLYP (no HF exchange).

4.1 Overall Performance

The performance of OCDFT on the full test set of first and second row core excitations with different functionals and basis sets is shown in Table 1. The data shows no dramatic difference in the accuracy of OCDFT regardless of the amount of Hartree-Fock (HF) exchange present in the functional. Even the "pure" DFT functional BLYP, shows comparable accuracy to its hybrid counterparts. BLYP often outperforms PBE0 and registers the same mean average error (MAE) as B3LYP across all basis sets. The Karlsruhe "def2" family of basis sets are built from the ground up to be a very uniform, widely applicable, economical choice of basis, and performs very well in this case. The correlation consistent (cc) basis sets also perform well, however are noticably more inaccurate than the def2 basis sets. The cc-pCVnZ family of basis sets were optimized to describe core-valence correlation effects for first row elements[39], since our test set includes excitations from second row elements these basis sets become noticably more inaccurate in those cases. Second row core electrons present unique challenges that we will consider in detail later in this section. Curiously, the cc-pCVQZ basis set performed the worst, which is surprising since basis sets generally become more accurate as they approach the complete basis set (CBS) limit.

Basis Set	Functional	MAE (eV)
def2-QZVP	B3LYP	1.0
	BLYP	1.0
	PBE0	1.4
def2-TZVP	B3LYP	1.0
	BLYP	1.0
	PBE0	0.9
cc-pCVTZ	B3LYP	1.3
	BLYP	1.3
	PBE0	1.6
cc-pCVQZ	B3LYP	1.5
	BLYP	1.5
	PBE0	1.7

Table 1 Mean absolute error in the core-excited states calculated using OCDFT on a test set of 35 different core excited states from 13 different molecules.

The average error of OCDFT is commensurate to wave-function methods that have been used to treat core-excited states. Asmuruf and Besley reported an average error of 1.2 eV for SOS-CIS(D) applied to a set of excitations similar to the ones used in the present study.[9] While Coriani et.al[8] reported errors of less than 0.9 eV when applying coupled cluster response theory to a set of carbon, nitrogen, and neon core excitations. These methods are still not as accurate as computations done on valence excitations, which often yield errors of less than 0.3 eV when using conventional CI or DFT methods.[CITE]

A full comparison of the accuracy of OCDFT and TDDFT over first row and second row core excitations is shown in the histogram in Fig. 2. OCDFT performs very well, peaking at an error close to zero and its largest error being -3.7 eVs. On the contrary, TDDFT performs rather poorly, peaking at an error close to -15 eVs and its largest error being -53.6 eVs.

Fig. 2 hints at a specific difficulty of conventional TDDFT. Notice the gap, roughly 15 eV wide, that exists between the two clusters of TDDFT data. This gap exists because TDDFT becomes sharply more inaccurate when dealing with second row core excitations. All of the TDDFT errors that are higher in magnitude than -20 eVs can be attributed to core

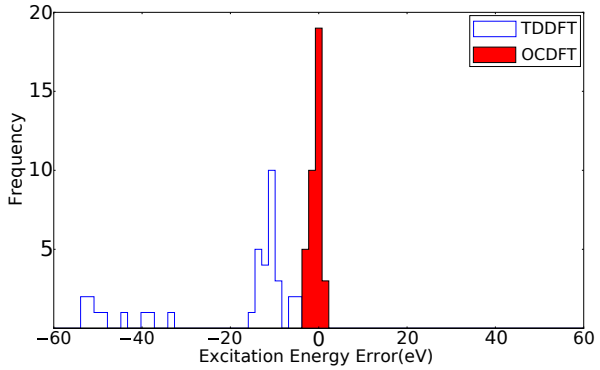

Fig. 2 Histogram showing the distribution of the error in the computed core excited states. All calculations were done using the B3LYP functional and the def2-QZVP basis set. The red filled bar is OCDFT while the empty blue bar is TDDFT.

excitations involving 1s orbitals located on second row nuclei. This dramatic drop in accuracy suggests that it is helpful to consider first row and second row core excitations seaparately to highlight the distinctive challenges that arise from each case.

4.2 First-Row Core Excitations

Table 2 shows valence and Rydberg excited states in which the core orbital is localized on a first row element, either C, N, or O 1s orbitals. Excitation energies were calculated using TDDFT and OCDFT in tandem with the B3LYP functional and basis sets of quadruple zeta quality. TDDFT produces a mean absolute error of 11.6 eVs compared to experiment, and as discussed earlier, this is consistent with previous studies that used TDDFT with a conventional hybrid functional [CITE]. OCDFT calculations under the same conditions yield a mean absolute error of 0.4 eV. To put this error into perspective, it can be compared to the performance of TDDFT with the $BH^{0.58}$LYP functional [CITE], a reparameterization of the BHLYP functional that has been augmented to include 58% HF exchange, 39% B88 exchange, and 8% Slater exchange. When applied to a test set similar to those in Figure 2, it yielded a mean average error of 0.8 eVs. A comparable level of accuracy was achieved by OCDFT without altering the inherent amount of HF exchange present in the functional.

It is customary to remedy the deficiency of TDDFT by shifting the position of the computed spectra by an amount that minimizes the difference between the computational and experimental peak features. In the case of the first row elements, this would imply shifting the TDDFT spectra by about 10 eV and using an even larger shift when dealing with heavier atoms. For example, a study done by DeBeer, Petrenko, and Neese[38] showed that it is necessary shift the TDDFT Fe K-edges of different iron complexes by 171.3 eV in order to correct the spectra. For OCDFT the computed excitation energies are in good agreement with experiment, making these arbitrary shifts unnecessary.

4.3 Second Row Core Excitations: Importance of Orbital Overlap

When computing core excited states of second row nuclei, TDDFT becomes highly inaccurate culminating in an average error above 30 eV after applying the DKH relativistic correction. Previous work by Tozer et al. showed that there is a relationship between the level of accuracy of TDDFT excitation energies and the amount of overlap between the orbitals involved.[CITE] This relationship should carry over to core electron excitations, where the core hole and valence particle

Molecule	Excitation	Exp.	def2-QZVP		cc-pCVQZ	
			TDDFT	OCDFT	TDDFT	OCDFT
CO	C 1s $\rightarrow \pi^*$	287.4	-11.3	-0.8	-10.9	0.9
	C 1s $\rightarrow$ 3s	292.4	-10.5	0.9	-10.8	1.2
	O 1s $\rightarrow \pi^*$	534.2	-13.4	-1.2	-14.4	-1.4
	O 1s $\rightarrow$ 3s	538.9	-13.0	0.2	-13.9	0.3
H_2CO	C 1s $\rightarrow \pi^*$	286.0	-10.7	-0.6	-10.7	-0.8
	C 1s $\rightarrow$ 3s	290.2	-10.7	-0.2	-10.7	-0.3
	O 1s $\rightarrow$ 3s	535.4	-14.1	-0.6	-14.1	-0.7
	O 1s $\rightarrow \pi^*$	530.8	-14.0	-0.8	-14.1	-1.1
$N_2O^\dagger$	O 1s $\rightarrow \pi^*$	534.8	-14.3	-1.0	-14.3	-1.3
	O 1s $\rightarrow$ 3s	536.7	-13.6	-0.4	-13.6	-0.6
	N_c 1s $\rightarrow$ 3s	407.5	-12.1	0.6	-12.6	0.6
	N_t 1s $\rightarrow \pi^*$	401.1	-12.2	-0.9	-14.6	2.5
	N_t 1s $\rightarrow$ 3s	404.0	-11.5	-0.4	-11.0	-0.5
N_2	N 1s $\rightarrow \pi^*$	401.0	-12.4	-0.9	-12.4	-1.1
	N 1s $\rightarrow$ 3s	406.2	-8.5	1.7	-7.2	2.7
HCN	C 1s $\rightarrow \pi^*$	286.4	-10.6	-0.5	-10.6	-0.7
	C 1s $\rightarrow$ 3s	289.1	-9.9	-0.1	-9.9	-0.3
	N 1s $\rightarrow \pi^*$	399.7	-12.0	-0.8	-12.0	-1.0
	N 1s $\rightarrow$ 3s	401.8	-10.4	0.2	-10.4	0.0
CH_4	C 1s $\rightarrow$ 3p	288.0	-10.1	0.1	-10.1	0.0
	C 1s $\rightarrow$ 3s	287.1	-10.8	-0.5	-10.8	-0.6
C_2H_2	C 1s $\rightarrow \pi^*$	285.8	-10.5	-0.1	-10.4	-0.7
	C 1s $\rightarrow$ 3s	287.7	-9.1	-0.6	-8.9	-0.3
	MAE		11.6	0.4	11.7	0.6

Table 2 Calculated core excitation energies for excitations involving 1s electrons of first-row atoms. Computations were performed using the B3LYP density functional, the values reported here are the deviations from the experimental value in electron volts (eV). Mean Absolute Error (MAE) is reported for each basis set.
†For N_2O the subscript c and t stand center and tail nitrogen respectively.

orbitals have little overlap, which decreases further when dealing with the hole and particle orbitals of second row nuclei. The overlap between the hole and particle orbital is defined by the following integral

$$\Lambda_{hp} = \int |\phi_h||\phi_p| \, d\tau, \tag{14}$$

which yields a unitless value between 0 (no overlap) and 1 (complete overlap) that describes the amount of overlap between the two orbitals involved. The scatterplot in Figure 3 displays the effect that a decrease in orbital overlap has on the performance of each method. The dashed line at 0.12 eV separates the low overlap region (containing exclusively excitations from second row 1s core orbitals) from the higher overlap region (containing exclusively excitations from first row 1s and second row 2p core orbitals). The scatterplot clearly shows that OCDFT is less sensitive to this drop in overlap. OCDFT becomes more inaccurate by only 1.5 eV, while TDDFT has a 35.9 eV increase in error.

Molecule	Excitation	Exp.	def2-QZVP		cc-pCVQZ	
			TDDFT	OCDFT	TDDFT	OCDFT
SiH_4	Si 1s $\rightarrow \sigma^*$	1842.5	-38.4	-1.8	-38.9	-2.3
	Si 2p $\rightarrow \sigma^*$	102.8	-4.8	0.6	-4.1	1.5
PH_3	P 1s $\rightarrow \sigma^*$	2145.8	-44.1	-2.9	-44.1	-3.2
	P 2p $\rightarrow \sigma^*$	132.3	-5.1	0.7	-5.1	0.0
H_2S	S 1s $\rightarrow \sigma^*$	2473.1	-48.3	-3.0	-48.3	-3.8
	S 1s $\rightarrow$ 4p	2476.3	-52.1	-1.5	-52.1	-0.6
	S 2p $\rightarrow \sigma^*$	164.5	-5.1	0.8	-5.1	0.4
	S 2p $\rightarrow$ 4s	166.5	-7.1	-0.7	-7.1	-1.0
SO_2	S 1s $\rightarrow \pi^*$	2473.8	-50.1	-3.7	-51.3	-4.5
	S 1s $\rightarrow$ 4p	2478.4	-49.3	-2.4	-50.4	-3.2
	S 2p $\rightarrow$ 4s	171.3	-8.3	-1.5	-8.2	-1.9
HCl	Cl 1s $\rightarrow \sigma^*$	2823.9	-53.8	-2.3	-55.4	-4.7
	Cl 1s $\rightarrow$ 4p	2827.8	-52.1	-0.7	-52.7	-1.7
	Cl 2p $\rightarrow \sigma^*$	201.0	-6.1	0.8	-6.1	0.3
Cl_2	Cl 1s $\rightarrow \sigma^*$	2821.3	-53.6	-1.6	-55.3	-3.6
	Cl 1s $\rightarrow$ 4p	2828.5	-51.7	0.9	-53.5	-0.2
	Cl 2p $\rightarrow \sigma^*$	198.7	-5.7	-0.8	-5.8	-0.3
	MAE		31.6	1.6	32.0	2.0

Table 3 Calculated core excitation energies for excitations involving 1s electrons of second-row atoms. Computations were performed using the B3LYP density functional, the values reported here are the deviations from the experimental value in electron volts (eV). Mean Absolute Error (MAE) is reported for each basis set.

4.4 Treatment of Highly Symmetric Molecules and Self Interaction

Treating core excited states in highly symmetric molecules presents a unique challenge for conventional DFT functionals that are based on the local density approximation (LDA). The existence of symmetry equivalent atoms becomes problematic for both pure and hybrid functionals due to the approximate treatment of exchange by the exchange-correlation functional.[CITE] Since exchange is approximated rather than treated exactly, the self-interaction error (SIE) present in the Coulomb integral becomes a quantitative problem. Self-interaction an unphysical phenomenon that results from the orbital density $|\phi_i|^2$ interacting with itself

$$\hat{J}_{ii} = \int |\phi_i|^2 \, \frac{1}{r_{ii}} \, |\phi_i|^2 \, d\tau. \tag{15}$$

Qualitatively, this happens in every computational method, however it only becomes a quantitative problem for DFT because exchange is approximated rather than handled exactly in the LDA. A classic example of this problem is the dissociation of the H_2^+ ion[CITE]. Due to the approximate treatment of exchange, conventional functionals converge on a solution that is lower than the true dissociation energy. To avoid this problem and obtain a state where the core hole is localized, we utilize a wavefunction with broken symmetry. In order to execute this we first do a ground state

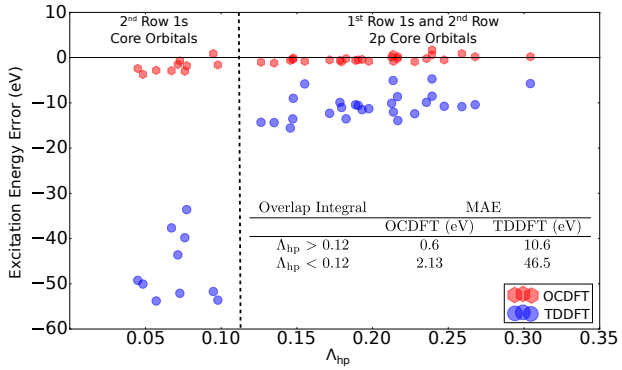

Fig. 3 Scatterplot displaying the excitation energy error as a function of orbital overlap. Excitation energies were calculated using the B3LYP functional and def2-QZVP basis set. The overlap integrals were computed with numerical grid integration making use of the Gaussian cube files produced by in Psi4 OCDFT calculations. Grids were calculated with a double zeta basis set and 0.1 grid spacing.

KS calculation imposing the full molecular point group, this yields the delocalized symmetry restricted solution. Using this as a starting point, another KS calculation is executed where the symmetry of the wavefunction is broken by mixing the columns of the alpha and beta coefficient matrices of the wavefunction leading to a reduction of symmetry, this yields the localized symmetry unrestricted solution. The subsequent excitation energies were calculated using the symmetry unrestricted solution. This method was applied to all highly symmetric molecules in the test set (N_2, C_2H_2, and Cl_2)

The approximate treatment of exchange plagues all density functional methods[CITE], self interaction errors have become commonplace and finding better approximations for exchange are necessary. The root of the problem can be understood by comparing the singlet excitation energy expression of CIS to TDDFT and OCDFT. In the CIS framework, the core excitation energy for a singlet state can be obtained in the following way

$$\omega_s^{CIS} = \hat{h}_\mathrm{h} - \hat{h}_\mathrm{p} + \hat{J}_\mathrm{hp} - \hat{J}_\mathrm{pp}. \tag{16}$$

The excitation energy for TDDFT differs from the CIS excitation energy by a term that includes nonlocal integrals that rely on both the hole and particle functions simulataneously

$$\begin{aligned}\omega_s^{TDDFT} &= \Delta_s^{CIS} + (1-a)[\hat{J}_\mathrm{ph} - \hat{J}_\mathrm{hh}] \\ &\quad + (1-a)[v_\mathrm{p}^x - v_\mathrm{h}^x],\end{aligned} \tag{17}$$

where v_i^x is the exchange potential and a is a parameter that weights the relative amount of DFT and HF exchange. The nonlocal $\hat{J}_\mathrm{ph}$ coulomb repulsion integral is problematic and leads to a poor description of the coulombic attraction that exists between a positively charged hole and a negatively charged particle. Thus it can not naturally describe core excitations, and relies instead on the varying of the a parameter to increase accuracy. The improved performance of OCDFT for core excited states is largely due to the local nature of the integrals involved. The excitation energy for OCDFT differs from CIS by a term that is composed of integrals that are localized on either the hole or the particle, which guarantees it will be exact for low orbital overlap systems

$$\begin{aligned}\omega_s^{OCDFT} &= \Delta_s^{CIS} + (1-a)[v_\mathrm{p}^x - v_\mathrm{h}^x + \frac{1}{2}\hat{J}_\mathrm{pp} - \frac{1}{2}\hat{J}_\mathrm{hh} \\ &\quad + \frac{1}{2}(\mathrm{hh}|\hat{f}_x|\mathrm{hh}) + \frac{1}{2}(\mathrm{pp}|\hat{f}_x|\mathrm{pp})],\end{aligned} \tag{18}$$

where $(\mathrm{ii}|\hat{f}_x|\mathrm{ii}) = \int |\phi_\mathrm{i}|^2 \ \hat{f}_x \ |\phi_\mathrm{i}|^2 \ d\tau$ are the exchange kernel integrals. The local nature of the integrals in this term provide a better approximation to exact exchange. This is a direct consequence of the orthogonality condition imposed between

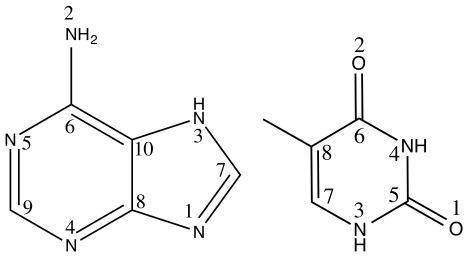

Fig. 4 Numbering scheme of adenine (left) and thymine(right), atoms are assigned a number based on increasing Hartree-Fock orbital energy of their 1s core orbital.

the ground and excited states, resulting in a term that is much more adept at handling systems with low orbital overlap. It has been concluded that varying HF exchange parameters can vastly improve the description of core-excited states, however here we approached the problem in a different way. With a slight augmentation to DFT derived from first principles, an accurate description of core excited states is possible without relying on varying the amount of HF exchange.

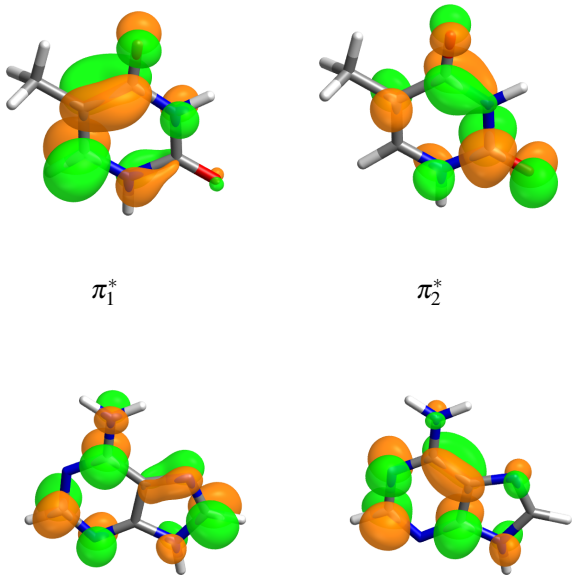

Fig. 5 Valence particle orbitals for thymine (top) and adenine (bottom) calculated using OCDFT with the B3LYP functional and def2-TZVP basis set.

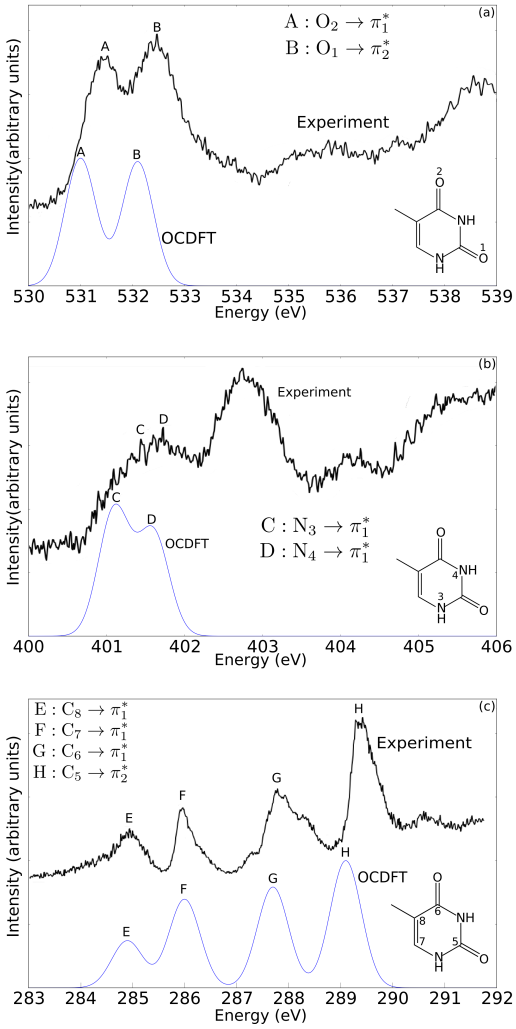

Fig. 6 Core excited states for thymine computed using B3LYP functional and def2-TZVP basis set. Spectra is composed of convoluted Gaussians with a Full Width at Half Maximum (FWHM) of 0.3 eVs of the (a) oxygen K-edge, (b) nitrogen K-edge, and (c) carbon K-edge. Experimental spectra is from reference [CITE].

4.5 Application to Nucleobases: Thymine and Adenine Near-Edge Spectra

The position of spectral features computed with OCDFT are in excellent agreement with experiment. At this time the limitations of the MCHP algorithm make it possible to only compute the valence states of a molecules like thymine and adenine with little to no symmetry. With the smaller,

Peak	Excitation	Exp.	OCDFT
A	$O_2 \rightarrow \pi_1^*$	531.4	531.0
B	$O_1 \rightarrow \pi_2^*$	532.3	532.1
C	$N_3 \rightarrow \pi_1^*$	401.7	401.6
D	$N_4 \rightarrow \pi_1^*$	401.5‡	401.1
E	$C_8 \rightarrow \pi_1^*$	284.9	284.9
F	$C_7 \rightarrow \pi_1^*$	285.9	286.0
G	$C_6 \rightarrow \pi_1^*$	287.8	287.7
H	$C_5 \rightarrow \pi_2^*$	289.4	289.1

Table 4 Calculated and experimental thymine core excitation energies in eV are shown in the table. All excitations originate from the 1s orbital on the specified atom.
‡Experimental value for this transition is inconclusive, value shown here was calculated using ADC(2)

symetrical molecules in our test set, it was possible to exploit symmetry in order to obtain the Rydberg states, but that isn't possible with nonsymmetrical molecules. However, since most K-edge spectra have strong features arising from excitations to valence antibonding orbitals[CITE], it is still possible to evaluate the accuracy of OCDFT in simulating spectral features. Theoretical line intensities were approximated using the oscillator stengths computed in OCDFT. The excited state orbitals shown in Figure 4 are the two unique molecular orbitals from thymine. The most likely excited state orbital chosen by the MCHP algorithm depends on the spatial orientation of the core orbital. Almost all core orbitals are excited to π_1^* while the 1s orbitals from O_1 and C_5 are excited to π_2^* using this procedure. Due to the projective nature of the algorithm, it is not possible to obtain the other valence states, Rydberg states, or mixed valence/Rydberg states without exploiting symmetry, which is not helpful for a molecule like Thymine. Thus at this time it is only possible to obtain the excitations from the respective 1s orbital and its closest valence orbital.

Figure 6 shows the oxygen, nitrogen, and carbon K-edge computed with OCDFT compared to NEXAS experiments done on gas-phase thymine performed by Plekan et al. [CITE] In this work, they also performed second-order algebraic-diagrammatic construction [ADC(2)] calculations to aid their experiment. Even while employing this highly sophisticated wavefunction method, in order to achieve optimal agreement with the experimental data they shifted the calculated spectra by a uniform value of -2.52 eV. Here we present spectra that have been computed using OCDFT and have not been shifted from their calculated value.

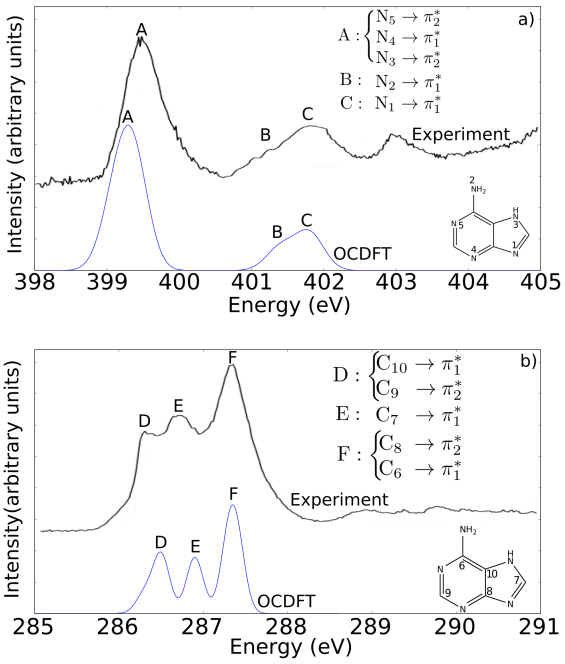

Fig. 7 Core excited states for adenine computed using B3LYP functional and def2-TZVP basis set. Spectra is composed of convoluted Gaussians with a FWHM of 0.2 eVs of the (a) nitrogen K-edge and (b) carbon K-edge.

The computed oxygen K-edge shown in Figure 6a is in good agreement with the experimental peaks. The two most dominant features of this spectra are excitations from the

Peak	Exp.	Excitation	OCDFT
A	399.5	$N_5 \rightarrow \pi_2^*$	399.4
		$N_4 \rightarrow \pi_1^*$	399.1
		$N_3 \rightarrow \pi_2^*$	399.3
B	401.3	$N_2 \rightarrow \pi_1^*$	401.4
C	401.9	$N_1 \rightarrow \pi_1^*$	401.8
D	286.4	$C_{10} \rightarrow \pi_1^*$	286.3
		$C_9 \rightarrow \pi_2^*$	286.5
E	286.8	$C_7 \rightarrow \pi_1^*$	286.9
F	287.4	$C_8 \rightarrow \pi_2^*$	287.4
		$C_6 \rightarrow \pi_1^*$	287.3

Table 5 Calculated and experimental adenine core excitation energies in eV are shown in the table. All excitations originate from the 1s orbital on the specified atom.

respective O 1s orbitals, to π^* particle orbitals. The MCHP algorithm is able to reproduce these features well. The energy region above 534 eV is dominated by Rydberg transitions and mixed valence/Rydberg states and therefore is outside the scope of the current study. The most prominent feature of the experimental N K-edge shown in Figure 6b is the large peak near 403 eVs. This peak is a mix of valence and Rydberg excitations from the N_3 1s and N_4 1s orbitals, however because of the projective nature of the algorithm we are unable to calculate these states at this time. Peak C at 401.6 eVs is in excellent agreement with the experimental peak maximum around 401.7 eVs. The N 1s excitation manifold is complex, the experimental spectra is cluttered with multiple transitions within a small region. This makes it difficult to clarify exactly which experimental peak that D corresponds to, but we can compare our value to the same transition calculated using ADC(2) (See table in Figure 4 for details). Figure 6c shows that the computed C K-edge is in excellent agreement with experimental spectra. All of the prominent features of this spectra are excitations from C 1s orbitals to the π^* particle orbitals. The computed line intensities are very similar to the experimental spectra giving us great confidence in the ability of OCDFT to compute the oscillator strengths of core-valence excited states.

Figure 7 displays the nitrogen and carbon K-edges of adenine computed with OCDFT. Peak A, the most prominent feature of the spectra, contains contributions from three of the nitrogen atoms located on the ring system. Since peak A is composed entirely of valence excitations from unique 1s core orbitals, this is the best glimpse at the accuracy of OCDFT when it is able to calculate all peak contributions. The peak of the Gaussian formed by all contributions to the peak is centered around 399.3 eV, very close to the experimental peak centered at 399.5 eV. The relative line intensity, when compared to peaks B and C, is almost identical to the relative intensity seen in the experimental spectra. Peak B is largely a shoulder feature of peak C, and this relationship is captured perfectly in our theoretical spectra. The experimental peak at 403 eV is composed of Rydberg excitations from N_3 and N_4, outside the scope of the MCHP algorithm. The carbon K-edge is also in good agreement, once again we see a spectra whose main features can be captured without considering the Rydberg states. The three main peaks between 286 eV and 288 eV are well represented by OCDFT. The line intensity of peak F is replicated well, although the intensities of peaks D and E differ slightly from experiment.

5 Conclusions

Orthogonality constrained density functional theory represents a new frontier in simulating excited states using density functional methods. Many of the efforts in this field have centered around developing new functionals in order to compensate for the shortcomings of the standard GGA functionals by varying the amount of hartree-fock exchange and other parameters present in the functional. However, here we show that standard functionals preform well with OCDFT at computing core-excited states due to the local nature of the integrals present in the excitation energy expression that allow for a better description of core-valence excitations. We have proven this by benchmarking OCDFT over a range of first and second row core excitations using standard pure and hybrid functionals. OCDFT showed no significant dependence on the amount of HF exchange, producing similar results across different functionals with varying fractions of HF exchange. OCDFT was also performed well across both the first and second row of the periodic table, only losing approximately 1.0 eV of accuracy when moving to the second row of the periodic table. Also outperforming TDDFT by 11.1 eV when calculating first row core excitations, and by 30.0 eV when calculating second row core excitations. We also calculate the nitrogen, oxygen, and carbon K-edges of thymine and adenine to show that OCDFT produces acceptable spectral profiles without the aid of an arbitrary energy shift.

Currently the biggest shortcoming of OCDFT is the limitations of the projective method to solving the Kohn–Sham equations. However this can be remedied by augmenting the code to allow for multiple projections from core orbitals. Once this is implemented, it should be possible to reproduce the complete NEXAS spectral profile of a system, this work is currently underway. Another area for improvement is to develop analytic energy gradients for OCDFT. This will allow us to study more complex systems and move beyond studying excited states and effectively study other molecular properties more throughly. We hope to present these extensions of this work in the near future.

References

1 E. M. McMillan, *Physical Review*, 1945, **68**, 143–144.

2 W. Hua, B. Gao, S. Li, H. gren and Y. Luo, *J. Phys. Chem. B*, 2010, **114**, 13214–13222.

3 G. Contini, V. Carravetta, V. Di Castro, S. Stranges, R. Richter and M. Alagia, *The Journal of Physical Chemistry A*, 2001, **105**, 7308–7314.

4 G. Hhner, *Chem Soc Rev*, 2006, **35**, 1244–1255.

5 Q. X. Guo, H. Senda, K. Saito, T. Tanaka, M. Nishio, J. Ding, T. X. Fan, D. Zhang, X. Q. Wang, S. T. Liu, B. Shen and R. Ohtani, *Applied Physics Letters*, 2011, **98**, 181901.

6 M. Feneberg, M. Rppischer, N. Esser, C. Cobet, B. Neuschl, T. Meisch, K. Thonke and R. Goldhahn, *Applied Physics Letters*, 2011, **99**, 021903.

7 T. Nakazato, M. Oyamada, N. Niimura, S. Urasawa, O. Konno, A. Kagaya, R. Kato, T. Kamiyama, Y. Torizuka, T. Nanba, Y. Kondo, Y. Shibata, K. Ishi, T. Ohsaka and M. Ikezawa, *Phys. Rev. Lett.*, 1989, **63**, 1245–1248.

8 S. Coriani, O. Christiansen, T. Fransson and P. Norman, *Physical Review A*, 2012, **85**, year.

9 F. A. Asmuruf and N. A. Besley, *Chemical Physics Letters*, 2008, **463**, 267–271.

10 J. A. Sheehy, T. J. Gil, C. L. Winstead, R. E. Farren and P. W. Langhoff, *The Journal of Chemical Physics*, 1989, **91**, 1796–1812.

11 N. A. Besley, A. T. B. Gilbert and P. M. W. Gill, *The Journal of Chemical Physics*, 2009, **130**, 124308.

12 L. Triguero, L. G. M. Pettersson and H. gren, *Phys. Rev. B*, 1998, **58**, 8097–8110.

13 M. Stener, G. Fronzoni and M. de Simone, *Chemical Physics Letters*, 2003, **373**, 115–123.

14 E. Runge and E. K. Gross, *Physical Review Letters*, 1984, **52**, 997.

15 M. R. Silva-Junior, M. Schreiber, S. P. A. Sauer and W. Thiel, *The Journal of Chemical Physics*, 2008, **129**, 104103.

16 A. Dreuw and M. Head-Gordon, *J. Am. Chem. Soc.*, 2004, **126**, 4007–4016.

17 G. Tu, Z. Rinkevicius, O. Vahtras, H. gren, U. Ekstrm, P. Norman and V. Carravetta, *Physical Review A*, 2007, **76**, year.

18 N. A. Besley, M. J. G. Peach and D. J. Tozer, *Physical Chemistry Chemical Physics*, 2009, **11**, 10350.

19 A. Nakata, Y. Imamura, T. Otsuka and H. Nakai, *The Journal of Chemical Physics*, 2006, **124**, 094105.

20 G. Capano, T. Penfold, N. Besley, C. Milne, M. Reinhard, H. Rittmann-Frank, P. Glatzel, R. Abela, U. Rothlisberger, M. Chergui and I. Tavernelli, *Chemical Physics Letters*, 2013, **580**, 179–184.

21 N. A. Besley and A. Noble, *The Journal of Physical Chemistry C*, 2007, **111**, 3333–3340.

22 N. A. Besley and F. A. Asmuruf, *Physical Chemistry Chemical Physics*, 2010, **12**, 12024.

23 F. A. Evangelista, P. Shushkov and J. C. Tully, *J. Phys. Chem. A*, 2013, **117**, 7378–7392.

24 P. W. Ayers, M. Levy and A. Nagy, *Physical Review A*, 2012, **85**, year.

25 F. Weigend and R. Ahlrichs, *Physical Chemistry Chemical Physics*, 2005, **7**, 3297.

26 F. Weigend, *Phys Chem Chem Phys*, 2006, **8**, 1057–1065.

27 J. M. Turney, A. C. Simmonett, R. M. Parrish, E. G. Hohenstein, F. A. Evangelista, J. T. Fermann, B. J. Mintz, L. A. Burns, J. J. Wilke, M. L. Abrams, N. J. Russ, M. L. Leininger, C. L. Janssen, E. T. Seidl, W. D. Allen, H. F. Schaefer, R. A. King, E. F. Valeev, C. D. Sherrill and T. D. Crawford, *WIREs Comput Mol Sci*, 2012, **2**, 556–565.

28 D. Maganas, M. Roemelt, T. Weyhermller, R. Blume, M. Hvecker, A. Knop-Gericke, S. DeBeer, R. Schlgl and F. Neese, *Physical Chemistry Chemical Physics*, 2014, **16**, 264.

29 S. DeBeer George and F. Neese, *Inorganic Chemistry*, 2010, **49**, 1849–1853.

30 M. Bauer, *Physical Chemistry Chemical Physics*, 2014, **16**, 13827.

31 A. L. Ankudinov, J. J. Rehr, J. J. Low and S. R. Bare, *The Journal of Chemical Physics*, 2002, **116**, 1911.

32 M. Levy, *Physical Review A*, 1995, **52**, R4313.

33 J. P. Desclaux, D. F. Mayers and F. O'brien, *Journal of Physics B: Atomic and Molecular Physics*, 1971, **4**, 631.

34 M. Douglas and K. M. Norman, *Quantum Electrodynamical Corrections to the Fine Structure of Helium*, 1973.

35 B. A. Hess, *Applicability of the no-pair equation with free-particle projection operators to atomic and molecular structure calculations*, 1985.

36 B. A. Hess, *Physical Review A*, 1986, **33**, 3742.

37 R. De Francesco, M. Stener, M. Caus?, D. Toffoli and G. Fronzoni, *Physical Chemistry Chemical Physics*, 2006, **8**, 4300.

38 S. DeBeer George, T. Petrenko and F. Neese, *J. Phys. Chem. A*, 2008, **112**, 12936–12943.

39 D. E. Woon and T. H. Dunning, *The Journal of Chemical Physics*, 1995, **103**, 4572.